Open Research Online

Source counts at 15 microns from the AKARI NEP survey

Journal Item

oro.open.ac.uk

Science with AKARI

Source counts at 15 microns from the AKARI NEP survey

C. P. Pearson[1,2,7], S. Oyabu[3], T. Wada[3], H. Matsuhara[3], H. M. Lee[4], S. J. Kim[4], T. Takagi[3], T. Goto[5,6], M. S. Im[4], S. Serjeant[7], M. G. Lee[4], J. W. Ko[4], G. J. White[7], and O. Ohyama[8]

[1] Space Science and Technology Department, CCLRC Rutherford Appleton Laboratory, Chilton, Didcot, Oxfordshire OX11 0QX, UK
e-mail: chris.pearson@stfc.ac.uk
[2] Department of Physics, University of Lethbridge, 4401 University Drive, Lethbridge, Alberta T1J 1B1, Canada
[3] Institute of Space and Astronautical Science, Yoshinodai 3-1-1, Sagamihara, Kanagawa 229 8510, Japan
[4] Department of Physics and Astronomy, Seoul National University, Shillim-Dong, Kwanak-Gu, Seoul 151-742, Korea
[5] Institute for Astronomy, University of Hawaii, 2680 Woodlawn Drive, Honolulu, HI, 96822, USA
[6] National Astronomical Observatory, 2-21-1 Osawa, Mitaka, Tokyo, 181-8588, Japan
[7] Astrophysics Group, Department of Physics, The Open University, Milton Keynes, MK7 6AA, UK
[8] Academia Sinica, Institute of Astronomy and Astrophysics, Taiwan

ABSTRACT

We present galaxy counts at 15 microns using the Japanese AKARI satelitte's NEP-deep and NEP-wide legacy surveys at the north ecliptic pole. The total number of sources detected are approximately 6700 and 10 700 down to limiting fluxes of 117 and 250 microJy (5 sigma) for the NEP-deep and NEP-wide survey respectively. We construct the Euclidean normalized differential source counts for both data sets (assuming 80 percent completeness levels of 200 and 270 microJy respectively) to produce the widest and deepest contiguous survey at 15 microns to date covering the entire flux range from the deepest to shallowest surveys made with the infrared space observatory (ISO) over areas sufficiently significant to overcome cosmic variance, detecting six times as many sources as the largest survey carried out with ISO. We compare the results from AKARI with the previous surveys with ISO at the same wavelength and the Spitzer observations at 16 microns using the peek-up camera on its IRS instrument. The AKARI source counts are consistent with other results to date reproducing the steep evolutionary rise at fluxes less than a milliJansky and super-Euclidean slopes. We find the the AKARI source counts show a slight excess at fluxes fainter than 200 microJanskys which is not predicted by previous source count models at 15 microns. However, we caution that at this level we may be suffering from the effects of source confusion in our data. At brighter fluxes greater than a milliJansky, the NEP-wide survey source counts agree with the Northern ISO-ELAIS field results, resolving the discrepancy of the bright end calibration in the ISO 15 micron source counts.

Key words. galaxies: evolution – infrared: galaxies – surveys

1. Introduction

Tiered cosmological surveys at infrared wavelengths are the most efficient method to collect data on large ensembles of dusty star-forming galaxies viewed and different cosmological epochs (i.e. different redshifts). Since the pioneering survey of IRAS (Soifer et al. 1987) more than two decades ago, a series of dedicated infrared missions have pushed our understanding of the dusty Universe to increasingly further cosmological distances. Although, IRAS discovered indications of a dusty evolving Universe, it was the deep mid-infrared surveys carried out with the ISO (Kessler et al. 1996), especially in the ISOCAM 15 μm band (e.g., Elbaz et al. 1999, 2005, and references therein), which revealed the true extent of the violent evolution underway in galaxies from redshifts 0.1−1. This evolution in the infrared galaxy population was confirmed by the later *Spitzer* space observatory surveys at 24 μm (Papovich et al. 2004) which also extended the observations of the evolution in the infrared galaxy population out to even higher redshifts of ~2.5, thus linking the local Universe to the distant high redshift ($z > 2.5$) Universe observed at submillimetre wavelengths

by SCUBA (e.g. Smail et al. 1997; Hughes et al. 1998; Blain et al. 1999a; Scott et al. 2002; Mortier et al. 2005)

The AKARI satellite was launched on board JAXA's M-V8 launch vehicle on February 22, 2006 Japan standard time, JST and is Japan's first space mission dedicated to infrared astrophysics (Murakami et al. 2007). The 68.5 cm cooled telescope directs light on to two focal plane instruments, the far-infrared surveyor (FIS) (Kawada et al. 2007) and the infrared camera (IRC) (Onaka et al. 2007). AKARI's orbit is Sun-synchronous which dictates that any large surveys can only be carried out at the ecliptic poles. The north ecliptic pole (NEP) was chosen as the site for AKARI's premier deep cosmological survey with the IRC instrument (The AKARI-NEP survey Matsuhara et al. 2006). The IRC consists of three cameras, the IRC-NIR, MIR-S & MIR-L with nine broad band photometric filters which cover the continuous wavelength from 2 to 26 μm, in the filter bands $N2(2.4\ \mu m)$, $N3(3.2\ \mu m)$, $N4(4.1\ \mu m)$, $S7(7.0\ \mu m)$, $S9W(9.0\ \mu m)$, $S11(11.0\ \mu m)$, $L15(15.0\ \mu m)$, $L18W(18.0\ \mu m)$, and $L24(24.0\ \mu m)$ respectively. The NEP survey has a "wedding cake" configuration with a central ~0.38 square degree deep circular area with ~2500 s exposures for each filter (The NEP-deep survey Wada et al. 2008), and a near concentric surrounding

shallower survey covering 5.8 square degrees with ~300 s exposures for each filter hereafter referred to as the NEP-wide survey Lee et al. (2008). The real strength of the AKARI NEP survey lies in the unprecedented photometric coverage from near to mid-infrared wavelengths, critically including the wavelength domain between *Spitzer*'s IRAC and MIPS instruments from $8 < \lambda < 24$ μm where only limited coverage is available (from the peek-up camera on the IRS, Teplitz et al. 2005). This multi-wavelength view provides a unique opportunity to study infrared luminous galaxies whose mid-infrared spectra are complicated by emission and absorption features i.e., the PAH lines and silicate absorption feature, etc.

In this work, we report on the IRC *L*15 15 μm band results in the AKARI NEP survey region. In Sect. 2 we summarize the observations and processing of the *L*15 band data. Source extraction, photometry and construction of the source counts is presented in Sect. 3. In Sect. 4 we compare the results of the AKARI *L*15 band survey with the previous surveys carried out by the ISO & *Spitzer* space observatories. A brief summary is given in Sect. 5. Throughout this work, a concordance cosmology of $H_0 = 72$ km s^{-1} Mpc^{-1}, $\Omega = 0.3$, $\Lambda = 0.7$ is assumed.

2. Observations and data reduction

2.1. The AKARI NEP large-area survey at 15 μm

The NEP survey was carried out as AKARI guaranteed time core observations referred to as a large-area survey (LS) program. The stipulation for the NEP survey was to cover a sufficient area to a sufficient depth to overcome the effect of cosmic variance on the resulting statistics (See Somerville et al. 2004, for discussion on cosmic variance; and Matsuhara et al. 2006, for the NEP survey design). The volume required to sufficiently overcome cosmic variance (achieve a variance <5−10%) transpires to areas of >0.5 square degrees for redshifts of >1 (the NEP-deep survey) and >5 square degrees for redshifts <1 (the NEP-wide survey). The observations were carried out throughout the mission lifetime over the period of May 2006 to August 2007. For the NEP-deep survey a total of 266 pointed observations were taken tracing out a central circular region with uniform coverage of ~0.38 square degrees centred on a position RA = 17h56m, Dec = 66d37m offset from the NEP, using the IRC astronomical observing template (AOT) designed for deep observations (IRC05). For each waveband a total of 4 pointings were made at each position. The details of the observation strategy for the NEP-deep survey are given in Wada et al. (2008). Note that the total area covered in the 15 μm band including all coverage around the periphery of the central region results in a total area of ~0.6 square degrees.

The NEP-wide survey consisted of a total of 446 pontings were made in a circular region covering 5.8 square degrees centred on the NEP (i.e. encompassing but slightly offset from the NEP-deep survey). To maximize the area and the number of wavebands, the shallower IRC03 observing template was used. A total of 3 pointings were made at each position. The details of the observation strategy for the NEP-wide survey are given in Lee et al. (2008).

2.2. Data reduction

The data for the NEP survey were reduced by the standard IRAF-based IRC imaging pipeline (version 20071017; see the IRC data user manual, Lorente et al. 2007). The pipeline corrects basic

Table 1. Summary of parameters used for source extraction.

Parameter	Value
Pixel scale	2.34 arcsec
Detection threshold	1.65
Number of pixels required above threshold	5
Aperture diameter	7.5 arcsec
Kron factor	2.5 arcsec
Minimum radius	3.5 arcsec
magnitude zero point	23.573

instrumental effects, performing dark subtraction, linearity correction, distortion correction and flat fielding for individual data frames. Removal of the diffuse background was achieved by subtracting the median filtered self-image from the observations.

Spurious events, such as cosmic rays were removed at the frame co-addition stage using a 3 sigma clipping technique. The average value for each pixel among the frames rather than the median value, was used in order to further improve the signal-to-noise of the final image. Individual frames are co-add together using associations with bright stars between frames to produce the final pointing image. Astrometry was added to the 15 μm image frames by comparing pointings with those taken at the the shorter, near-infrared AKARI wavebands (the near-infrared AKARI wavebands have astrometry added by comparison with the 2MASS catalogue).

The individually processed pointings were then mosaiced together using the publicly available software SWarp[1] to produce the final mosaiced image. A detailed account of the data reduction is given in Wada et al. (2008).

3. Source counts
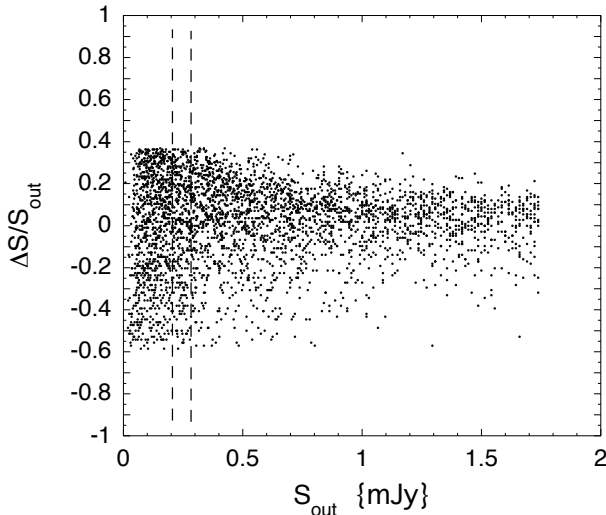
3.1. Source extraction and photometry

Sources were extracted from the final NEP-deep and NEP-wide images using the SExtractor software (Bertin & Arnouts 1996) with the criteria of five connected pixels in the image map having more than a 1.65σ signal above the local background, corresponding to a 5σ detection for a uniformly distributed flux. Photometry was carried out using SExtractor's MAGAUTO variable elliptical aperture size technique with the aperture parameters Kron factor and minimum radius set to their default values of 2.5 and 3.5, respectively and with the magnitude zero point derived from observations of standard stars (Tanabe et al. 2008). The source extraction parameters are summarized in Table 1. Aperture corrections were estimated by carrying out fixed aperture size photometry at different apertures from 5.0, 6.0, 9.0, 12.0, 15.0, 20.0 arcsecs using SExtractor's MAGAPER function. In Fig. 1 we show the result of the source extraction to the the 5σ level of the NEP survey using the MAGAPER and MAGAUTO parameters in SExtractor. The MAGAPER assumes apertures equal to the same aperture radius of standard stars used for the flux calibration while the MAGAUTO fits the best elliptical aperture. It was found that with the aperture set to the same size as used for the standard star observations (7.5 pixels for the *L*15 band image), that both aperture techniques were consistent with each other and that no aperture correction was necessary.

In Fig. 2 we create a simulation to check the photometric accuracy of our source extraction. Artificial sources are input to the image and then extracted using the same source extraction procedure as used for the real data. The value $\Delta S/S_{out}$ is plotted as a

---

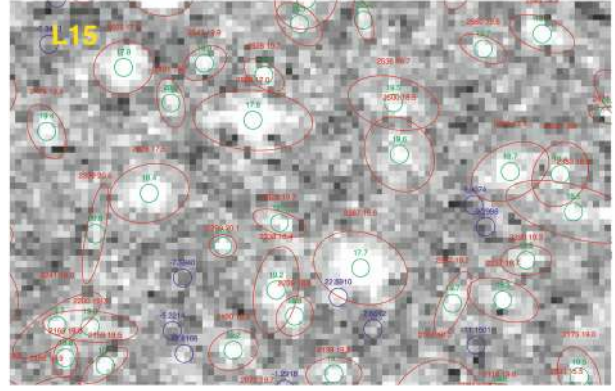[1] http://terapix.iap.fr/rubrique.php?idrubrique=49
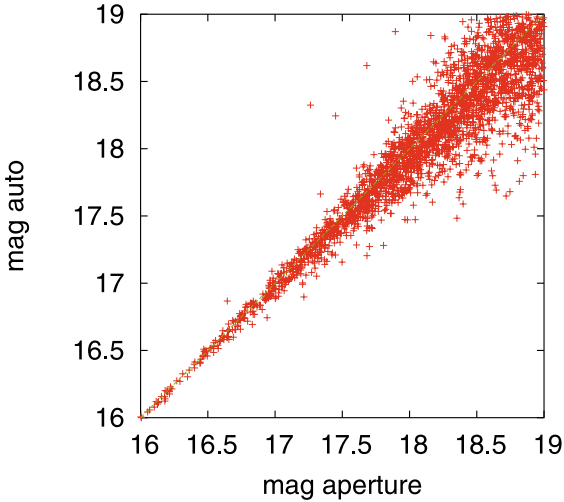
Fig. 1. The result of the source extraction using the MAGAPER and MAGAUTO parameters in SExtractor. The MAGAPER assumes apertures equal to the same aperture radius of standard stars used for the flux calibration while the MAGAUTO fits the best elliptical aperture.
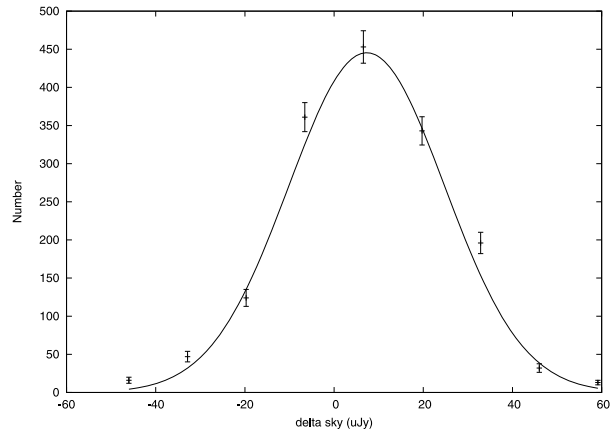

Fig. 3. A segment of the AKARI NEP-deep survey field showing the typical distribution of sources. The small circles mark the position of the sources where the peak flux is measured. The larger surrounding ellipses are the MAGAUTO apertures. The smaller isolated circles not on a source are areas of blank sky measurements.


Fig. 4. The noise histogram for the AKARI NEP survey. The measured points are well fitted by a Gaussian with a tail to positive fluxes indicative of a faint source population (contributing to the confusion).

Fig. 2. A simulation of the photometric accuracy of our source extraction. The fractional difference in the flux $\Delta S / S_{out}$ ([output–input]/output) as a function of the measured flux density. Also shown are the 80% completeness limits from Sect. 3.3.

function of the measured flux density where ΔS is the difference between the recovered flux and input flux. We find a dispersion of $15-30\%$ is seen from bright to fainter fluxes. These values are consistent with the expected flux accuracy of the IRC processing pipeline (Lorente et al. 2007). Also shown in the figure are the 80% completeness limits from Sect. 3.3.

Figure 3 shows a segment of the AKARI NEP deep survey field showing the typical distribution of sources. We find that in almost all cases that the sources are sufficiently separated as to avoid any significantly effects from blending. Calibration of the source fluxes was made using the conversion factors given in the the IRC data user manual (Lorente et al. 2007). The final source catalogues consist of a total of 6737 and 10 686 sources detected at 15 μm in the NEP-deep and NEP-wide surveys respectively. The noise was estimated by measuring the fluctuations at random blank sky positions (See Fig. 3). Positions close to sources were avoided to ensure no contamination from the sources themselves. We made simple aperture photometry at each random

position using the IRAF/PHOT package. The size of aperture radius was set to 1.5 pixels with no weighting or PSF fitting assumed. In order to evaluate the fluctuations in the photometry, the noise histogram was fit with a Gaussian distribution. We defined the one sigma level of the fluctuation as the standard deviation. The noise histogram is shown in Fig. 4. Note the positive tail corresponding to faint sources.

3.2. Raw source counts

To calculate the raw source counts from of catalogue we bin the data in flux bins of $\Delta \lg S = 0.08$. The resulting raw count histogram is shown in the *left* panel of Fig. 5 for the NEP-deep survey and the *right* panel for the NEP-wide survey. For the NEP-deep survey, a total of 6737 sources are detected with a 5σ flux limit of $\sim117\,\mu$Jy (i.e. detected as 5σ sources above the noise), although sources are extracted to an order of magnitude deeper. We observe a peak in the raw counts histogram between $50-100\,\mu$Jy. For the NEP-wide survey a total of 10 686 sources are detected at a 5σ limit of $\sim250\,\mu$Jy (although the raw numbers were extracted to an order of magnitude deeper). The peak of the distribution, around a milli-Jansky, is somewhat narrower than the NEP-deep survey.
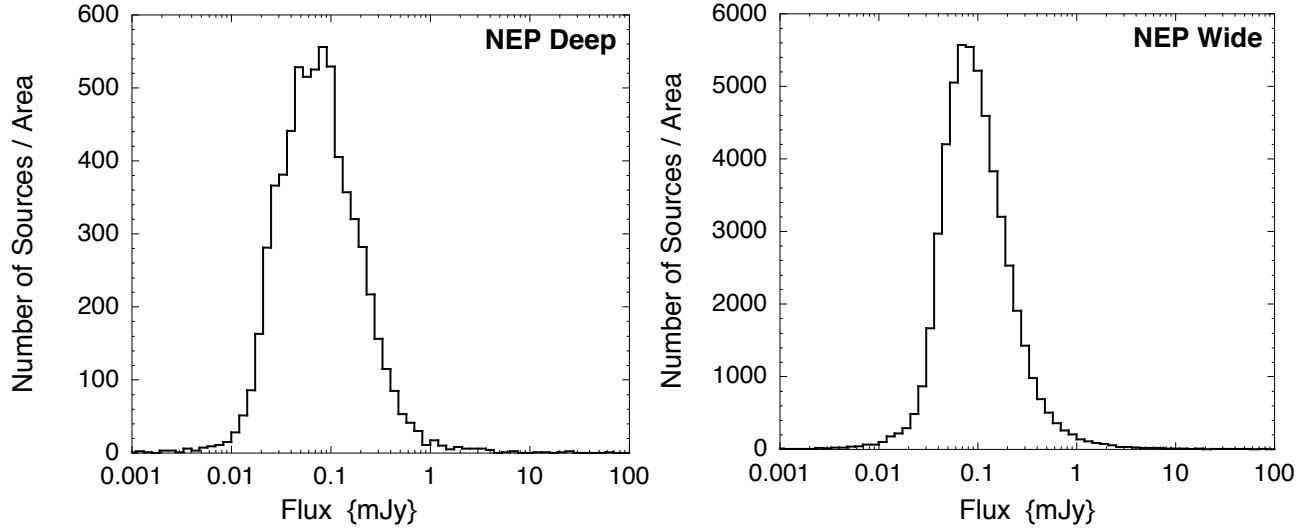
Fig. 5. Raw source counts for the *left* AKARI NEP-deep survey and *right* NEP-wide survey in the *L*15 (15 μm) band. Differential histogram of the number of sources detected in a flux bin of size $\Delta \lg S = 0.08$.

3.3. Completeness, reliability, and stellar fractions

The method used for the correction of any incompleteness in the data has been described in detail in Wada et al. (2008). The completeness was calculated from Monte Carlo simulations by injecting artificial sources into the map at known positions and then performing the same source extraction to recover the sources. The flux range was divided into logarithimic flux bins of equal size and populated with 20 sources assuming a Euclidean Universe distribution and a circular PSF. The completeness fraction as a function of flux is then given by the ratio of the number of true sources extracted to the total number of input sources. For each bin, five independent simulations were made resulting in around 100 sources per flux bin. The final completeness for the survey is shown in Fig. 6 for the NEP-deep survey (*left panel*) and NEP-wide survey (*right panel*) respectively. From the figures, we find 50% completeness limits of ~100 μJy and 150 μJy and 80% completeness limits of ~200 μJy and 270 μJy for the NEP-deep and NEP-wide surveys respectively.

The reliability of the detections has been checked by carrying out the same source extraction on the negative images and calculating the fraction of these spurious sources detected to the number of real sources detected on the positive image as a function of flux. The results are shown in Fig. 7 for the fraction of spurious detections. We find that the NEP-deep survey is expected to be highly reliable at both the 50% and the 80% completeness level. However, in the case of the NEP-wide survey, the survey is only 50% reliable (following this definition of reliability) at the 50% completeness level. At the 80% completeness level the NEP-wide survey is >75% reliable. As an additional reliability check, the overlapping regions of the NEP-deep and -wide surveys were also examined by eye to confirm the reality of sources in both images. We find that the NEP-wide sources can be reliably identified with NEP-deep counterparts down to a flux limit of ~250 μJy which is brighter than the measured 50% completeness limit of 150 μJy discussed above. Therefore we assume the 80% completeness limit numbers for our source count analysis.

Stellar fractions were calculated using the optical data taken by the Canada France Hawaii Telescope (CFHT) and Near-Infrared data taken by the Kitt Peak National Observatory (KPNO) over the NEP-wide region (which also encompasses

Table 2. Fraction of stellar contribution to source counts.

| lg (Flux) (mJy)	Stellar fraction
1.272	0.5
1.072	0.35
0.872	0.286
0.672	0.20
0.472	0.136
0.272	0.135
0.072	0.133
−0.128	0.093
−0.328	0.091
−0.528	0.082
−0.728	0.063
−0.928	0.054

the NEP deep region, Hwang et al. 2007). The AKARI 15 μm sources were cross matched with CFHT/KPNO data, with stellar sources have stellarity >0.8 and optical *r'* band magnitudes <19 identified during the source extraction. The stellarity was checked via colour-magnitude and colour−colour diagrams. It is found that almost all the star-like sources have bright AKARI *L*15 band AB magnitudes <14 while the extragalactic sources lie at magnitudes >14. The stellar sources can also be clearly segregated using the stellarity >0.8 and optical *r'* band magnitudes <19 and the near-infrared colour criteria of $H - N2 < -1.6$ in the $H - N2$, $g - H$ colour plane (where $N2$ is the AKARI IRC 2.5 μm band). We have also checked our stellar criteria in the $H - L15$ versus H Color−Magnitude diagram (similar to Shupe et al. 2008, but with somewhat different filter bands). Our criteria agree well (within a few %) and therefore is regarded as sufficient in statistically correcting for stellar sources. In Table 2 the stellar fraction as a function of flux (bins of lg $(S/\text{mJy}) = 0.2$) is shown, the star counts are also shown in Fig. 8.

3.4. Confusion and clustering

At the faint fluxes probed by the NEP-deep survey, confusion – defined as the flux limit below which sources are indistinguishable from the background noise becomes an important limiting factor. Confusion noise is a function of the beam size
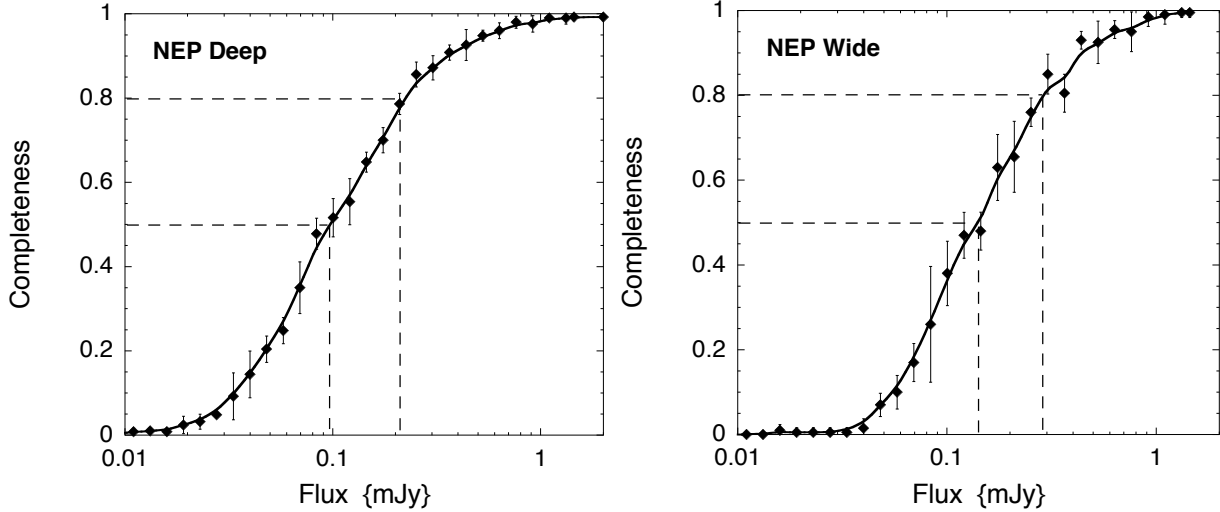
Fig. 6. 5σ completeness function for the AKARI NEP survey in the $L15$ (15 μm) band for the *left* AKARI NEP-deep survey and *right* NEP-wide survey. The best fit curve to the data and the 50% and 80% completeness levels are also shown.
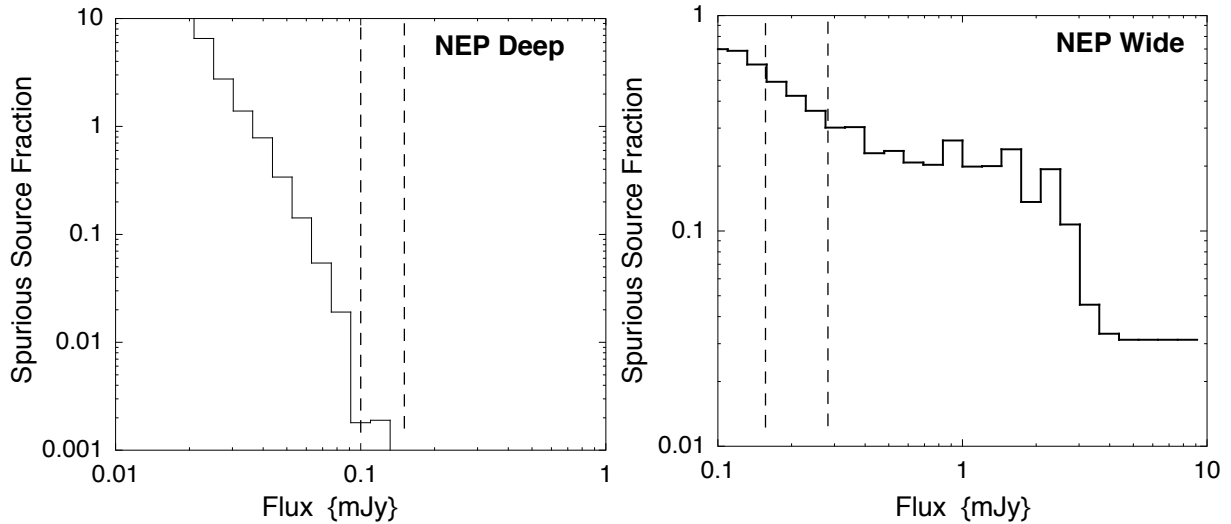

Fig. 7. A measure of the reliability of the NEP surveys measured by examining the fraction of spurious sources detected from the negative image of the the *left* AKARI NEP-deep survey and *right* NEP-wide survey. The 50% and 80% completeness levels are also shown for comparison.

of the telescope and is thus worse at longer wavelengths and smaller apertures. Classically, the confusion limit is defined at the level where one source occupies a beam but practically the confusion limit is often set to 20−50 beams per source (Hogg 2001; Condon 1974). For ISO Oliver et al. (1997) carried out a $P(D)$ analysis of the ISO-HDF observations which did not use a source detection algorithm but rather looked for fluctuations in the background caused by sources around or below the confusion limit in the survey. A clear, positive signal was indeed detected in the data and interpreted as the contribution from faint galaxies. Oliver et al. (1997) concluded that for ISO, a 60 cm diameter telescope, the confusion limit due to point sources was ∼200 μJy. For AKARI, a 70 cm diameter telescope, the classical confusion limit of 50 beams per source is predicted to be ∼100 μJy using the models of Pearson (2005). However at the faint sensitivities of the NEP-deep survey, where the source counts are strongly non-Euclidean the classical beams per source criteria may not be accurate. To investigate the confusion limit of the NEP survey

we carried out a measurement of the beam to beam fluctuations in the noise as a function of flux (e.g. Jeong et al. 2006; Dole et al. 2003; Vaisanen et al. 2001) by defining the signal to noise, $q = S_{lim}/\sigma_c(S_{lim})$, as the ratio of the flux limit to the rms noise measured from beam to beam fluctuations due to sources fainter than the flux limit. The equation is solved iteratively with values for q usually chosen to be between 3−5. We find values of $S_{lim} = 25−53$ μJy for $q = 3$ and 5 respectively. Wada et al. (2008) have calculated the number of sources per beam for the NEP-deep survey finding that for the $L15$ band there is an average of 1/53.7 sources per beam at the 5σ detection limit of 117 μJy. This value of 53.7 beams per source is close to the classical confusion limits quoted by Hogg (2001) and Condon (1974).

We have also used the source density criterion as detailed by, Jeong et al. (2006), Dole et al. (2003) for the case where the fluctuations are not the dominant contribution to the confusion but rather the the high density of resolved sources around the sensitivity limit (as is the case in the mid-infrared, e.g.
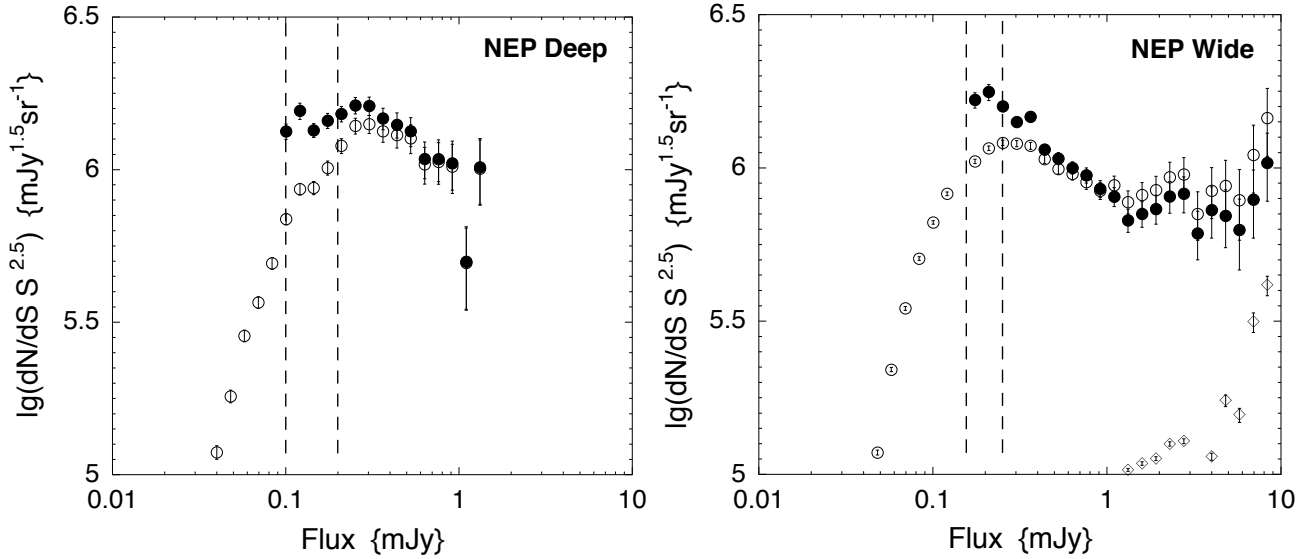
Fig. 8. Completeness corrected differential source counts (*filled circles*) normalized for a Euclidean Universe in the AKARI *L*15 band for the *left* NEP-deep survey and *right* NEP-wide survey. The vertical dashed lines show the 50% and 80% completeness levels from Fig. 6. The raw data is shown as *unfilled circles*. Also shown for the NEP-wide survey are the stellar counts (*unfilled diamonds*).

Dole et al. 2004; Rodighiero et al. 2006). In order to find the flux limit where the source detection becomes affected by confusion due to near neighbours we set the constraint of 80% completeness and use simulations to calculate $S_{\rm lim}$ and calculate the corresponding fluctuations at that level. The simulations yield confusion limits of ~130 μJy higher than the values from the fluctuation criteria alone but consistent with the 53.7 beams per source value of Wada et al. (2008) and closer to the theoretical prediction using the models of Pearson (2005).

Note that the AKARI NEP surveys are specifically designed to overcome major effects of cosmic variance including the effect of clustering on the counts (See Sect. 2.1). Although an analysis of the clustering properties of the NEP field is beyond the scope of this paper and will be presented in later work, we note that the amplitude due to clustering in the *Spitzer* 24 μm surveys has been found to be of the order of 0.0009−0.01 for $S_{24} > 350$ μJy (Magliocchetti et al. 2007, 2008), where the amplitude A is related to the angular correlation function $w(\theta) = A\theta^{1-\gamma}$, where θ is the angular separation on the sky and γ is the clustering index. Takeuchi et al. (2001) have shown that the errors on the number counts due to clustering depend on the angular correlation function and the area of the survey and provide a formulation for the signal to noise given by $S/N = \sqrt{\Omega / \int w(\theta) d\Omega}$, where Ω is the solid angle of the survey. Using this formulation we find errors on the number counts due to clustering between 3−9% for redshifts <1.6.

3.5. Final L15 band source counts

Using the results from Sect. 3.3 we present the completeness and stellar corrected normalized differential source counts per steradian ($(dN/dS)S^{2.5}$ in the units of mJy$^{1.5}$) in the AKARI *L*15 15 μm band in Fig. 8 for the NEP-deep survey (*left panel*) and NEP-wide survey (*right panel*) respectively. The Euclidean normalized differential sources are characterized by a flat distribution at bright fluxes, since the counts are normalized to a flux, $S^{2.5}$. Any evolution will present itself as an upturn in the counts at fainter fluxes and the counts will eventually tail off to fainter fluxes as cosmological redshift dimming takes effect. The

counts are plotted for fluxes brighter than the 50% completeness limit of ~100 μJy and 150 ~ 100 μJy for the NEP-deep and NEP-wide surveys respectively although the counts are assumed to be actually reliable at the 80% completeness limits of ~200 μJy and 270 ~ 100 μJy We also show the original raw source counts corrected to be counts per steradian and the star counts in the NEP-wide plot for comparison. At flux densities $1 < S < 10$ mJy the source counts are Euclidean in nature as expected. We see the characteristic evolutionary rise at fluxes below 1 mJy producing super-Euclidean slopes as seen in the ISO 15 μm surveys (Fadda et al. 2004; Metcalfe et al. 2003; Gruppioni et al. 2002; Altieri et al. 1999; Aussel et al. 1999). The differential source counts in the AKARI *L*15 band begin to rise from the Euclidean case around a flux of a mJy with the peak occuring between flux densities $0.25 < S < 0.3$ mJy. At fainter flux densities (<0.2 mJy) the source counts begin to fall away. The completeness corrected normalized differential source counts, $dN/dS.S^{2.5}$, from Fig. 8, are tabulated in Tables 3 and 4 for the NEP-deep and NEP-wide surveys respectively for the 50% completeness limit. Note that by summing the differential counts to obtain the integral number counts, we find that the NEP-wide source counts brighter than a milli-Jansky exhibit a slope of around 1.5, i.e. consistent with the non-evolving Euclidean Universe while at fainter fluxes both the NEP-wide and -deep counts are above Euclidean expectations.

4. Analysis

4.1. Comparison with other surveys

The wavelength regime on or around 15 μm has enjoyed copious coverage by both the ISO & *Spitzer* observatories. The surveys carried out by ISO-ISOCAM at 15 μm covered survey areas from ~0.001−10 square degrees to depths of 0.1−0.5 mJy. Although *Spitzer* strictly did not have imaging capability between the IRAC 8 μm band and the MIPS 24 μm band, it did have the potential for limited photometry at 16 μm (and 22 μm) using the "Peek Up Imaging" (PUI) mode on the Infrared Spectrograph (IRS) instrument (Houck et al. 2004).

Table 5 lists the major surveys to date carried out with the AKARI, ISO and *Spitzer* satellites. The table lists surveys by

Table 3. AKARI band NEP-deep survey $L15$ band Euclidean normalized differential source counts.

lg (Flux)	Counts	Errors	
	dN/d$S.S^{2.5}$	(low)	(high)
(mJy)	(mJy$^{1.5}$ sr^{-1})	(mJy$^{1.5}$ sr^{-1})	
0.121839	6.007522	5.886836	6.101860
0.041839	5.698483	5.542632	5.812936
−0.038160	6.020391	5.932722	6.093298
−0.118160	6.034276	5.960460	6.097348
−0.198160	6.034723	5.970412	6.090726
−0.278161	6.125328	6.075381	6.170118
−0.358161	6.146805	6.103473	6.186158
−0.438161	6.167757	6.131282	6.201397
−0.518161	6.208664	6.177380	6.237808
−0.598160	6.210495	6.182887	6.236405
−0.678160	6.182443	6.156610	6.206784
−0.758161	6.160284	6.135064	6.184017
−0.838161	6.128609	6.105217	6.150735
−0.918160	6.192664	6.164233	6.218212
−0.998160	6.125141	6.098685	6.149198

Table 4. AKARI band NEP-wide survey $L15$ band Euclidean normalized differential source counts.

lg(Flux)	Counts	Errors	
	dN/d$S.S^{2.5}$	(low)	(high)
(mJy)	(mJy$^{1.5}$ sr^{-1})	(mJy$^{1.5}$ sr^{-1})	
0.92184	6.1625	6.0376	6.2594
0.84184	6.0425	5.9176	6.1394
0.76184	5.8945	5.7637	5.9949
0.68184	5.9408	5.8365	6.0249
0.60184	5.9256	5.8344	6.0008
0.52184	5.8498	5.7632	5.9219
0.44184	5.9788	5.9160	6.0336
0.36184	5.9697	5.9150	6.0182
0.28184	5.9278	5.8781	5.9724
0.20184	5.9118	5.8679	5.9518
0.12184	5.8909	5.8517	5.9268
0.041839	5.9481	5.9161	5.9779
−0.038160	5.9315	5.9030	5.9582
−0.11816	5.9758	5.9501	5.9999
−0.19816	6.0000	5.9797	6.0193
−0.27816	6.0305	6.0103	6.0495
−0.35816	6.0603	6.0454	6.0746
−0.43816	6.1664	6.1502	6.1817
−0.51816	6.1496	6.1345	6.1637
−0.59816	6.2009	6.1884	6.2128
−0.67816	6.2476	6.2193	6.2716
−0.75816	6.2219	6.1947	6.2451
−0.83816	6.2994	6.2790	6.3175

mission, then by decreasing areal coverage. The characteristic sensitivity and total number of sources detected is also tabulated. We also give some representation of the co-moving volume encompassed by each survey by assuming the spectrum of the archetypical starburst galaxy M 82 at a luminosity of $L_{IR} \sim 10^{11} L_\odot$ and using the redshift at which this galaxy could be detected in each survey to calculate the corresponding volume.

The largest 15 μm survey carried out with ISO was the ELAIS survey (Rowan-Robinson et al. 2004; Vaccari et al. 2005; Pozzi et al. 2003). The resulting catalogue consisted of 1546 sources detected with $S/N > 5$ in the 0.5−100 mJy flux range over a total area of 10.3 square degrees in five fields ($N1$, $N2$, $N3$, $S1$, $S2$). ELAIS is best compared with the AKARI NEP-wide survey covering around half the area but to a factor

of two – three deeper in flux, detecting more than six times the number of sources. The superior depth of NEP-wide should enable the detection of $L_{IR} > 10^{11} L_\odot$ luminous infrared galaxies out to a redshift of unity compared to $z \sim 0.4−0.5$ for the ELAIS survey.

The AKARI NEP-deep survey is almost as deep as the very deepest surveys carried out with ISO in the lensed cluster fields (Altieri et al. 1999; Metcalfe et al. 2003). However, the cosmological volume sampled by the NEP-deep survey is thirty-seven times larger resulting in the detection of 1000's rather than 10's of sources, without the constraint of any complicated lens corrections.

Surveys of the *Hubble* deep fields (HDF), North and South have been carried out by *Spitzer* (and previously by ISO) using the IRS-PUI at 16 μm. (Teplitz et al. 2005, b). These observations, along with the AKARI PV-phase observations of Wada et al. (2007) are the deepest 15 μm observations to date reaching to depths of 40−90 μJy (but see Hopwood 2010, for deeper initial results with AKARI). However, the areas covered are tiny (10−150 square arcmins) and corresponding volumes (<0.2 Mpc^3) subject to the effects of cosmic variance (Somerville et al. 2004).

4.2. Comparison with observed source counts

In Fig. 9 we compare the results from the AKARI NEP-deep and -wide surveys with the observed source counts from the various surveys carried out by the ISO & *Spitzer* observatories at 15 μm. The figure shows the normalized differential counts per steradian showing that the AKARI source counts are in general agreement with the differential source counts at 15 μm to date, reproducing the upturn at around a milli-Jansky and the bump at around the 0.3 mJy level. However, the fainter end of the AKARI differential source counts falls off significantly slower than the corresponding *Spitzer* observations (Note that the *Spitzer* counts have not been corrected for completness). The results from the NEP-deep survey exhibit the same excess at fainter fluxes detected in the AKARI NEP PV-phase observations by Wada et al. (2007). The AKARI counts are more consistent (but still somewhat higher) with the deepest lensed surveys carried out with ISO Altieri et al. (1999).

At bright fluxes, the AKARI NEP-wide source counts provide a new constraint on the bright end source counts. Note that at fluxes of 1−10 mJy, the ISO source counts in the ELAIS-S field Gruppioni et al. (2002) are systematically lower than the Northern ELAIS fields and the fainter ISO surveys (Serjeant et al. 2000; Vaisanen et al. 2002; Rodighiero et al. 2004). Vaisanen et al. (2002) put this discrepancy down to calibration issues with the ISOCAM data and corrected the ELAIS-N source counts down by a factor of ~1.75. However, even after this correction, a significant discrepancy remains. In this work, the AKARI NEP-wide data appears to be more consistent with the results from the ELAIS-N surveys with the source counts lying significantly above the results from the ELAIS-S fields. The resolution of this discrepancy is an important issue for galaxy evolution modelling which relies on the bright end of the source counts to set the normalization of the models.

4.3. Comparison with evolutionary models

In Fig. 9 we also compare the observed counts with three contemporary galaxy evolution models. We overplot the evolutionary models of Lagache et al. (2004), Pearson (2005) and

Table 5. Comparison of major surveys carried out at 15 μm listed by mission, then by decreasing areal coverage.

Satellite	Survey	Area (deg^2)	Sensitivity (mJy)	Sources (number)	Volume (Mpc^3)
AKARI	NEP-wide[1]	5.8	0.25*	10686	57.2
AKARI	NEP-deep[2]	0.6	0.1*	6737	6.17
AKARI	NEP-PV[3]	0.02	0.07	277	0.21
AKARI	Abell 2218[4]	0.034	0.042	565	0.35
Spitzer	HDF-S[5]	0.04 (0.003)	0.09 (0.04)	515	0.41 (0.031)
Spitzer	HDF-N[6]	0.01	0.08	153	0.1
ISO	ELAIS S1[7]	4.17	0.5	736	38.86
ISO	ELAIS N1[7]	2.67	0.5	490	24.88
ISO	ELAIS N2[7]	2.67	0.5	566	24.88
ISO	ELAIS N3[7]	0.88	0.5	131	8.2
ISO	Lockman hole shallow[8]	0.55	0.25	457	5.41
ISO	Marano deep[9]	0.25	0.3	180	2.44
ISO	Lockman hole deep[10]	0.14	0.2	283	1.39
ISO	ELAIS S2[11]	0.12	0.4	43	1.15
ISO	CFRS 1452 field[12]	0.028	0.4	41	0.27
ISO	Marano UDSR[9]	0.025	0.3	142	0.244
ISO	Marano UDSF[9]	0.025	0.3	137	0.244
ISO	A370 cluster[13]	0.009	0.2	20	0.09
ISO	HDF-S[14]	0.008	0.25	24	0.079
ISO	HDF-N[15]	0.007	0.2	19	0.069
ISO	A2218 cluster[13]	0.006	0.1	46	0.062
ISO	A2390 cluster[16]	0.0015	0.1	34	0.015

Notes. (*) 5σ sensitivity above the noise.
References. [1] Lee et al. (2008); [2] Wada et al. (2008); [3] Lee et al. (2008); [4] Hopwood (2010); [5] Teplitz et al. (2005); [6] Teplitz et al. (2005); [7] Vaccari et al. (2005); [8] Fadda et al. (2004); [9] Elbaz et al. (1999); [10] Rodighiero et al. (2004); [11] Pozzi et al. (2003); [12] Flores et al. (1999); [13] Metcalfe et al. (2003); [14] Oliver et al. (2002); [15] Serjeant et al. (1997); [16] Altieri et al. (1999).

Rowan-Robinson et al. (2009) along with the non-evolving model of Pearson (2005). The evolution in the 15 μm source counts is immediately apparent by comparison with the no-evolution model of Pearson (2005) which falls off steeply at bright ($S > 10$ mJy) flux levels. All of the three evolutionary models fit the location of the peak flux in the 15 μm counts over the $0.2 < S < 0.4$ mJy range. The Lagache et al. (2004) model over predicts the AKARI counts at all fluxes brighter than 0.2 mJy and has a high normalization at the bright end. This model does fit the counts from the ISO deep surveys, however it should be noted from Table 5 that the AKARI NEP-deep Survey covers $1-2$ orders of magnitude larger area and should provide a more reliable estimate of the source counts at any given flux level. The model of Pearson (2005) produces a good fits to both the faint (<1 mJy) ISO & *Spitzer* counts and is consistent with the AKARI NEP-deep counts down to the 200 μm level. At fainter fluxes the predicted source counts fall off faster than the AKARI data. The model has a slightly lower normalization compared to the AKARI NEP-wide and ISO ELAIS-N counts at fluxes brighter than 200 mJy due to the necessity to strike a compromise between the normalization between the ELAIS-N and ELAIS-S counts. Although the Rowan-Robinson et al. (2009) model fits the AKARI source counts reasonably well at the sub-mJy level, the model misses the upturn in the flux at $S \sim 1-2$ mJy. All three models diverge at the faintest fluxes ($S < 0.1$ mJy) where the source counts are not well constrained and where the effects of galaxy confusion dominate.

5. Summary

We have derived the source counts at 15 μm from AKARI-IRC *L*15 band observations of the AKARI large-area survey at the North Ecliptic Pole. Source counts from both the NEP-deep

survey, (covering a larger area of ~0.6 square degrees compared to the uniform survey area of 0.38 square degrees reported in Wada et al. 2008) and the NEP-wide survey, covering 5.8 square degrees are presented. The total number of sources detected are 6737 and 10 700 down to 5σ limiting fluxes of 117 and 250 μJy for the NEP-deep and NEP-wide survey respectively.

The Euclidean normalized differential source counts have been shown for both surveys and we have compared the AKARI results with the previous surveys carried out at or around 15 μm with the ISO and *Spitzer* observatories. The 15 μm AKARI data cover the entire flux range from the deepest to shallowest ISO and *Spitzer* surveys (40 μJy->10 mJy) over areas sufficiently significant to overcome cosmic variance in the resulting statistics detecting six times as many sources as the widest surveys carried out with ISO.

The AKARI data is consistent with the evidence of strong evolution appearing in the source counts at fluxes of around a milli-Jansky and the super-Euclidean slopes observed in the differential sources counts at sub-milliJansky levels. At fainter fluxes the AKARI data is consistent with the ISO and *Spitzer* source counts down to fluxes of 200 μJy, reproducing the turnover in the differential source counts around 300 μJy. However, at the faintest fluxes (<200 μJy), the AKARI source counts fall off much slower than observed in the *Spitzer* data or predicted by evolutionary models, although the counts are still marginally consistent with the deep lensed differential counts from ISO. At these levels, confusion noise due to crowded fields may be becoming significant, affecting both the source extraction and the completeness corrections, and we estimate a confusion limit of ~130 μJy. Further processing of the data, including multi-wavelength source counts from the final band merged
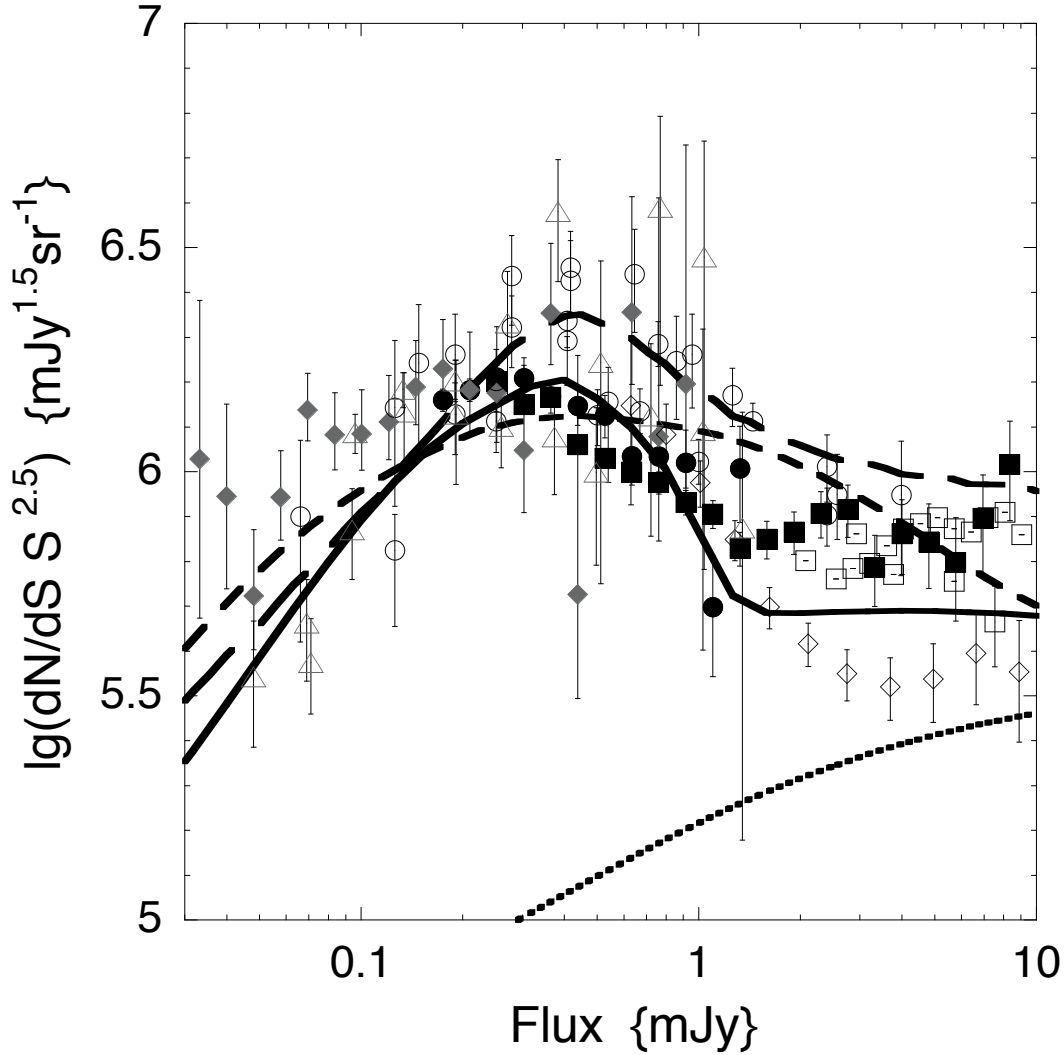
Fig. 9. Comparison of the AKARI-NEP survey *L*15 band differential source counts with the observational result of the surveys carried out at 15 µm by ISO & *Spitzer*. The AKARI NEP-deep obseervations are shown as *filled circles* and the AKARI NEP-wide observations as *filled squares*. Also plotted are the 15 µm differential source counts from the *Spitzer*/IRS GOODS-N & GOODS-S surveys *open triangles*, Teplitz et al. (2005), Teplitz (2005); deep ISO surveys of *open circles*, Altieri et al. (1999), Oliver et al. (1997), Aussel et al. (1999), Elbaz et al. (1999); ISO ELAIS-N *open squares*, Serjeant et al. (2000); ISO ELAIS-S *open diamonds* Gruppioni et al. (2002). In addition, for reference we plot the galaxy evolution models of Pearson (2005) as *dotted* (no-evolution scenario) and *solid* (evolving scenario), the models of Rowan-Robinson (2009) *dashed* line, and the models of Lagache (2004) as a *dot-dash* line.

catalogue will help to determine whether the faint excess is a real effect or an artifact of the source extraction in crowded fields.

At brighter fluxes, the NEP-wide data provides vital information on the bright-end normalization of the source counts at 15 µm, given the uncertainty in the calibration of the ISO source counts at fluxes brighter than a milliJansky. We find that the NEP-wide source counts converge to a flat Euclidean distribution more consistent with the ISO ELAIS-N source counts than the ELAIS-S field, even after the calibration corrections suggested by Vaisanen et al. (2002).

We have compared the source counts from the AKARI NEP survey with three contemporary galaxy evolution models, finding that the Lagache et al. (2004) model over predicts the AKARI source counts at all flux levels and the Rowan-Robinson et al. (2009) model misses the upturn of the source counts at 1−2 mJy. The model of Pearson (2005) fit both the magnitude and position of the the upturn in the source counts and the peak between $0.2 < S < 0.4$ mJy but has a slightly lower normal-

ization at the brightest fluxes compared to the NEP-wide counts. All three models diverge from each other at fainter fluxes where the source counts become confusion dominated.

References

Altieri, B., Metcalfe, L., Kneib, J. P., et al. 1999, A&A, 343, L65
Aussel, H., Cesarsky, C. J., Elbaz, D., et al. 1999, A&A, 342, 313

Bertin, E., & Arnouts, S. 1996, A&AS, 117, 393
Blain, A. W., Kneib, J.-P., Ivison, R. J., et al. 1999a, ApJ, 302, 632
Condon, J. J. 1974, ApJ, 188, 279
Chary, R., Casertano, S., Dickinson, M. E., et al. 2004, ApJSS, 154, 80
Dole, H., Lagache, G., & Puget, J.-L. 2003, ApJ, 585, 617
Dole, H., Reike, G. H., Lagache, G., et al. 2004, ApJ, 154, 93
Elbaz, D. 2005, Space Sci. Rev., 119, 93
Elbaz, D., Cesarsky, C. J., Fadda, D., et al. 1999, A&A, 351, L37
Fadda, D., Lari, C., Rodighiero, G., et al. 2004, A&A, 427, 23
Flores, H., Hammer, F., Thuan, T. X., et al. 1999, ApJ, 517, 148
Gruppioni, C., Lari, C., Pozzi, F., et al. 2002, MNRAS, 335, 831
Hogg, D. W. 2001, AJ, 121, 1207
Hopwood, R., Serjeant, S., Negrello, M., et al. 2010, AKARI Conf. Proc.,
    in press [arXiv:0912.2103]
Houck, J. R., Roellig, T. L., van Cleve, J., et al. 2004, ApJSS, 154, 18
Hughes, D., Serjeant, S., Dunlop J., et al. 1998, Nature, 394, 241
Hwang, N., Lee, M.G., Lee H.M. et al., 2007, ApJS, 172, 583
Jeong, W.-S., Pearson, C. P., Lee, H. M., et al. 2006, MNRAS, 369, 281
Kawada, M., Baba, H., Barthel, P. D., et al. 2007, PASJ, 59, 389
Kessler, M. F., Steinz, J. A., Anderegg, M. E., et al. 1996, A&A, 315, L27
Lagache, G., Dole, H., Puget, J.-L., et al. 2004, ApJS, 154, 112
Lee, H. M., Kim, S. J., Im, M., et al. 2009, PASJ, 61, 375
Lorente, R., Onaka, T., Ita, Y., et al. 2007, AKARI IRC data user manual, ver. 1.3
Magliocchetti, M., Silva, L., Lapi, A., et al. 2007, MNRAS, 375, 1121
Magliocchetti, M., Cirasuolo, M., McLure, R. J., et al. 2008, MNRAS, 383, 1131
Matsuhara, H., Wada, T., Matsuura, S., et al. 2006, PASJ, 58, 673
Metcalfe, L., Kneib, J.-P., McBreen, B., et al. 2003, A&A, 407, 791
Mortier, A. M. J., Serjeant, S., Dunlop, J. S., et al. 2005, MNRAS, 363, 563
Moshir, M., Kopan, G., Conrow, T., et al. 1990, Infrared Astronomical Satellite
    Catalog, Faint Source catalog version 2.0
Murakami, H., Baba, H., Barthel, P. et al., 2006, PASJ, 59, 369

Oliver, S. J., Goldschmidt, P., Franceschini, A., et al. 1997, MNRAS, 289, 471
Oliver, S. J., Mann, R. G., Carballo, R., et al. 2002, MNRAS, 289, 471
Onaka, T., Matsuhara, H., Wada, T., et al. 2007, PASJ, 59, 401
Papovich, C., Dole, H., Egami, E., et al. 2004, ApJSS, 154, 70
Pearson, C. P. 2005, MNRAS, 358, 1417
Pozzi, F., Ciliegi, P., Gruppioni, C., et al. 2003, MNRAS, 343, 1348
Pozzi, F., Ciliegi, P., Gruppioni, C., et al. 2004, MNRAS, 609, 122
Rodighiero, G., Lari, C., Fadda, D., et al. 2004, A&A, 427, 773
Rodighiero, G., Lari, C., Pozzi, F., et al. 2006, MNRAS, 371, 1891
Rowan-Robinson, M. 2009, MNRAS, 394, 117
Rowan-Robinson, M., Lari, C., Perez-Fournon, I., et al. 2004, MNRAS, 351,
    1290
Rush, B., Malkan, M., & Spinoglio, L. 1993, ApJS, 89, 1
Scott, S. E., Fox, M. J., Dunlop, J. S., et al. 2002, MNRAS, 331, 817
Serjeant, S. B. G., Eaton, N., Oliver, S. J., et al. 1997, MNRAS, 289, 457
Serjeant, S., Oliver, S., Rowan-Robinson, M., et al. 2000, MNRAS, 316, 768
Smail, I., Ivison, R. J., & Blain, A. W. 1997, ApJ, 490, L5
Soifer, B. T., Houck, J. R., & Neugebauer, G. 1987, ARA&A, 25, 187
Somerville, R. S., Lee, K., Ferguson, H. C., et al. 2004, ApJ, 600, L171
Takeuchi, T. T., Ishii, T. T., Hirashita, H., et al. 2008, PASJ, 60, 375
Tanabe, T., Sakon, I., Cohen, M., et al. 2001, PASJ, 53, 37
Takagi, T., Matsuhara, H., Wada, T., et al. 2007, PASJ, 59, 557
Teplitz, H. I. 2005, in When UV meets IR: a History of Star Formation, XXVth
    Moriond Astrophysics Meeting, La Thuile, Italy, March 6−12, ed. D. Elbaz,
    & H. Aussel
Teplitz, H. I., Charmandaris, V., Chary, R. R., et al. 2005, ApJ, 634, 128
Vaccari, M., Lari, C., Angeretti, L., et al. 2005, MNRAS, 358, 397
Vaisanen, P., Tollestrup, E. V., & Fazio, G. G. 2001, MNRAS, 325, 1241
Vaisanen, P., Morel, T., Rowan-Robinson, M., et al. 2002, MNRAS, 337, 1043
Wada, T., Oyabu, S., Ita, Y. et al., 2007, PASJ, 59, 515
Wada, T., Matsuhara, H., Oyabu, S., et al. 2007, PASJ, 59, 515